Reactive Power Control for Single-phase Grid-tie Inverters using Quasi Sinusoidal Waveform

Dong Li, Carl N.M. Ho, Luo Liu,
Department of Electrical & Computer Engineering,
University of Manitoba,
Winnipeg, Manitoba, Canada.
carl.ho@umanitoba.ca

Gerardo Escobar
School of Engineering,
Universidad Autonoma de Yucatan,
Merida, Yucatan, Mexico.
gescobar@ieee.org

***Abstract*— This paper presents a reactive power control technique for single-phase Photovoltaic (PV) inverters, especially unfolding inverter. The proposed system retains the benefit of the unfolding inverters having low BOM cost and semiconductor losses, and tackles the drawback of the standard unfolding inverter not having capability of reactive power injection. It is important to note that reactive power delivery is mandatory for PV inverters according to the recent announced regulations. The concept is based on changing the shape of the grid current waveform but keeping the same zero crossing points as in the unity power factor condition. The current waveform is governed by real power and reactive power, at the price of an acceptable deformation. The operating principles of the proposed technique and mathematical derivations of the grid current function are provided in the paper. Experimental results in a grid-tie inverter prototype have shown a good agreement with the derived theory, and they confirm the feasibility of using the proposed technique in grid-tie inverters.**

Keywords*— Photovoltaic, Inverter, Reactive Power, Power Factor

I. INTRODUCTION

Unfolding grid-tie inverters are generally used in Photovoltaic (PV) and Fuel Cell (FC) applications [1]-[8]. This is because a simple controller can be applied and it can minimize the number of high frequency switching semiconductors, e.g. MOSFETs. This leads to low component cost and high efficiency. Fig. 1 shows a typical system block diagram of an unfolding grid-tie inverter [3]. The front stage is a dc-dc converter, which converts a dc current from a voltage source to a rectified sinusoidal inductor current. The second stage is a line frequency inverter to unfold the inductor current into a bipolar sinewave current, which is synchronized with the grid voltage [9]-[11]. Typically, semiconductor switches in the line frequency inverter are SCR thyristors [9]. It is well-known that SCR are turned off at zero current with relatively long commutation time which makes difficult for the injection of reactive power. Thus, the impossibility of injecting reactive power is the main drawback of unfolding inverters. However, a new regulation has been recently published to require that PV inverter products must have the capability to adjust Power Factor (PF) up to 0.95 in either inductive or capacitive modes [12]. In consequence, a lot of already designed commercial products are facing the problem of not passing such a regulation. They have to change the topology of PV products.

The work described in this paper was fully supported by a grant from the Canada Research Chairs, Canada (Sponsor ID: 950-230361).

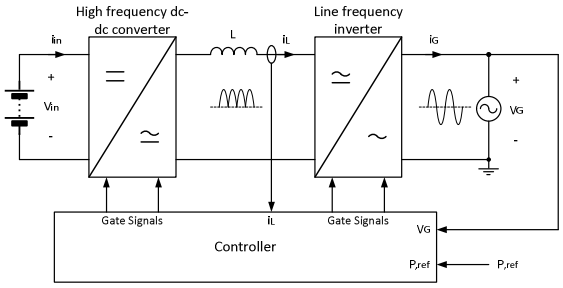

Fig. 1 A typical single-phase grid-tie unfloding inverter system.

Beside the regulation, unfolding inverters give a high efficiency when using MOSFETs in the line frequency inverter stage instead of SCRs. A commercial single phase PV inverter system can achieve 97.8% European efficiency with using Silicon MOSFETs only in the inverter stage [13]. The MOSFETs effectively reduce the conduction loss comparing to SCRs. However, the zero crossing points of grid current and gird voltage have to be synchronized, otherwise it will produce a short circuit path by the body diodes, otherwise, a series blocking diode is required for each MOSFET. The high efficiency advantage does not exist anymore due to a high conduction loss at the diodes [14]. Nevertheless, reactive power cannot be delivered to the grid. A manufacturer has provided a solution which changes the shape of the gird current waveform to give a capability of generating 0.95 power factor [15]. However, there are no further literatures to provide the operating principles and the performance evaluations by using the method.

This paper follows up the idea in the literature [15] to propose a control technique for grid-tie inverters, especially unfolding inverter. It modifies the delivered grid current with this paper proposed Quasi Sinusoidal Waveform (QSW) in such a way to deliver reactive power, and thus satisfying the PF regulations. The modified current keeps the same zero crossing points as the grid voltage. The injection of reactive power is thus possible at the expenses of an acceptable current shape deformation. Although it contains harmonics during reactive power delivering, the total harmonic distortion (THD) is minimized. Recall that, during unity power factor, the current satisfies the THD regulation such as IEEE519. This paper provides the mathematical derivation of the proposed grid current reference function. Numerical and experimental results of the proposed technique applied to an grid-tie inverter are presented to verify the theoretical findings.

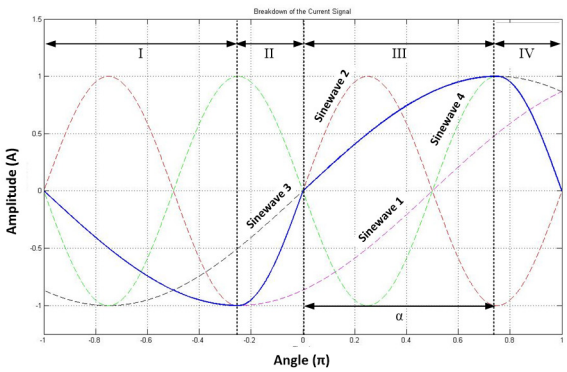

Fig. 2 Proposed Quasi Sinusoidal Waveform.

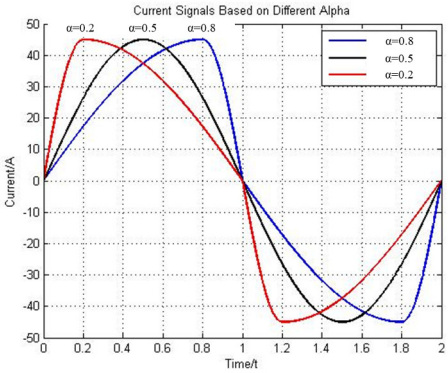

Fig. 3 Quasi Sinusoidal Waveform with different α.

II. Steady State Characteristics

A. Ideal Quasi Sinusoidal Waveform

In this paper, Quasi Sinusoidal Waveform (QSW) is defined as a waveform which is formed by sinusoidal waveforms with different frequencies. The resultant waveform is close to a sinewave but it includes harmonics in the signal. Fig. 2 shows the proposed QSW signal, which is proposed as the reference for the delivered grid current. This waveform is divided into 4 time intervals, where the boundaries are fixed at peaks and zero crossings of sinewaves. Notice that each interval consists of a fraction of a sine function whose frequency alternates between two different values. The mathematical expression of such a composed function is given by,

$$f(t)=\begin{cases}-\mathrm{A}\sin\dfrac{\pi\left(t+\frac{T}{2}\right)}{\alpha\mathrm{T}}, & -\dfrac{\mathrm{T}}{2}\le \mathrm{t} < -(1-\alpha)\dfrac{\mathrm{T}}{2}\\ \mathrm{A}\sin\dfrac{\pi t}{(1-\alpha)\mathrm{T}}, & -(1-\alpha)\dfrac{\mathrm{T}}{2}\le \mathrm{t} < 0\\ \mathrm{A}\sin\dfrac{\pi t}{\alpha\mathrm{T}}, & 0\le \mathrm{t} < \alpha\dfrac{\mathrm{T}}{2}\\ -\mathrm{A}\sin\dfrac{\pi\left(t-\frac{T}{2}\right)}{(1-\alpha)\mathrm{T}}, & \alpha\dfrac{\mathrm{T}}{2}\le \mathrm{t} < \dfrac{\mathrm{T}}{2}\end{cases} \quad (1)$$

where α adjust the shape of the curve and is referred as adjusting ratio. For instance, in Fig. 2, α is set to 0.75. A is peak value and T is period. Fig. 3 shows QSW signals with different α. Notice that, for $\alpha = 0.5$, a regular sinusoidal waveform is generated, otherwise the peaks of the waveform are shifted.

The frequency of sinusoidal wave in each interval can be determined by total QSW signal frequency f_Q and α as,

$$f_{\mathrm{I}} = f_{\mathrm{III}} = \frac{f_Q}{2\alpha} \quad (2)$$

and

$$f_{\mathrm{II}} = f_{\mathrm{IV}} = \frac{f_Q}{2(1-\alpha)} \quad (3)$$

These two variables, α and A, in (1) are used to adjust power factor and current amplitude of a current injecting into a grid. Fig. 3 shows a QSW with different α. When α is 0.5, it is a pure sinusoidal waveform, otherwise the peaks of the waveform are shifted. In the graph can be seen that the resultant frequency, and zero crossing points of waveforms are the same.

B. Fourier Series of Quasi Sinusoidal Waveform

In order to determine the periodic signal function of the QSW, the method of Fourier series is used [16]. The general equation of a Fourier series is,

$$f(t) = a_0 + \sum_{n=1}^{\infty}\left(a_n\cos\frac{2n\pi t}{T} + b_n\sin\frac{2n\pi t}{T}\right) \quad (4)$$

By considering the function in Eqn. (1) and Fig. 2, a_0 is equal to 0 due to no dc offset in the waveform, a_n and b_n can be determined by,

$$a_n = \frac{2A}{\pi}\cdot\frac{[1-(-1)^n]\cdot(2\alpha-1)}{[4n^2(\alpha-1)^2-1]\cdot(4n^2\alpha^2-1)}\cdot[1-4n^2\alpha(\alpha-1)-2n\sin(\alpha n\pi)] \quad (5)$$

$$b_n = \frac{2A}{\pi}\cdot\frac{[1-(-1)^n]\cdot(2\alpha-1)}{[4(\alpha-1)^2n^2-1]\cdot(4\alpha^2n^2-1)}\cdot 2n\cos(\alpha n\pi) \quad (6)$$

Therefore, based on Eqns. (4), (5) & (6) with angular frequency (ω), the current reference, $i(t)$, with QSW can be represented by the following equation,

$$i(t) = \sum_{n=1}^{\infty}(a_n\cos n\omega t + b_n\sin n\omega t) \quad (7)$$

where n is the number of harmonic of the current.

A periodic signal can be expanded to a fundamental frequency and harmonics. The general form is represented by,

$$i(t) = \sum_{n=1}^{\infty} I_n\sin(n\omega t + \theta_n) \quad (8)$$

where I_n is magnitude and θ_n is phase angle. Eqn. (8) can be further expanded as,

$$i(t) = \sum_{n=1}^{\infty} I_n(\sin\theta_n\cos n\omega t + \cos\theta_n\sin n\omega t) \quad (9)$$

By comparing Eqns. (7) and (9), two equations can be found as follows,

$$a_n = I_n\sin\theta_n \quad (10)$$

and

$$b_n = I_n\cos\theta_n \quad (11)$$

By putting (5) and (6) into (10) and (11), respectively, two equations can be obtained,

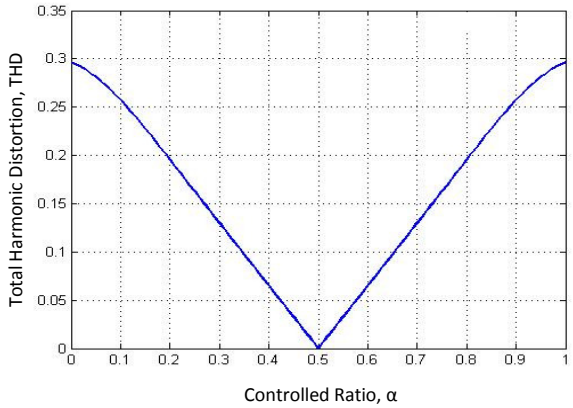

Fig. 4 THD changes based on different α.

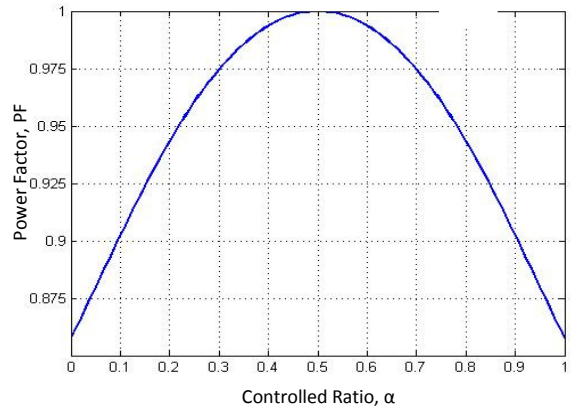

Fig. 5 Power factor changes based on different α.

$$I_n \sin\theta_n = \frac{2A}{\pi} \cdot \frac{[1-(-1)^n]\cdot(2\alpha-1)}{[4n^2(\alpha-1)^2-1]\cdot(4n^2\alpha^2-1)} \cdot [1 - 4n^2\alpha(\alpha-1) - 2n\sin(\alpha n\pi)] \quad (12)$$

$$I_n \cos\theta_n = \frac{2A}{\pi} \cdot \frac{[1-(-1)^n]\cdot(2\alpha-1)}{[4(\alpha-1)^2n^2-1]\cdot(4\alpha^2n^2-1)} \cdot 2n\cos(\alpha n\pi) \quad (13)$$

Magnitudes and phase angles of each harmonic of the signal can be calculated by assigning A and α with solving the equations of (12) and (13).

C. Electrical Characteristics

Furthermore, Total Harmonic Distortion (THD), Power Factor (PF), Real Power (P) and Reactive Power (Q) can be determined based on the parameters of the fundamental component and harmonic components of the current reference.

1) Total Harmonic Distortion (THD) and Power Factor (PF)

The equations for total harmonic distortion (THD) [17] and power factor (PF) [18] are,

$$THD = \frac{\sqrt{\sum_{n=3}^{\infty} I_n^2}}{I_1} \quad (14)$$

$$PF = \frac{1}{\sqrt{1+THD^2}} \cos\theta_1 \quad (15)$$

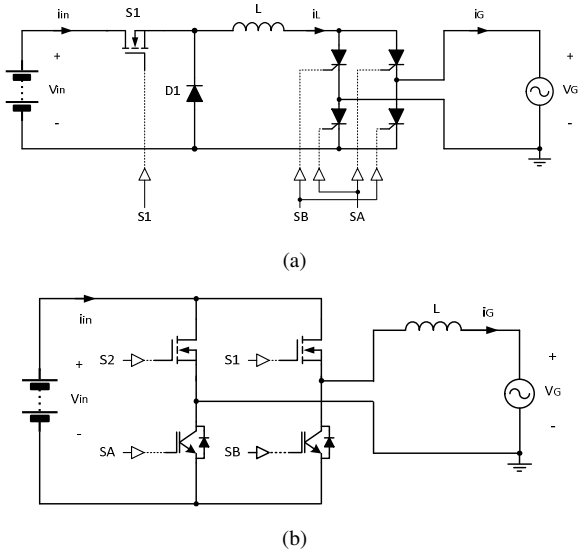

Fig. 6 Typical grid-tie inverter topologies: (a) unfolding inverter, and (b) unipolar switching full-bridge inverter.

By putting (13) with $n = 1$, and (14) into (15), the PF equation can be rewritten as,

$$PF = \frac{1}{\sqrt{\sum_{n=1}^{\infty} I_n^2}} \cdot \frac{4A\cdot(2\alpha-1)}{\pi[4(\alpha-1)^2-1]\cdot(4\alpha^2-1)} \cdot 2\cos(\alpha\pi) \quad (16)$$

Fig. 4 and Fig. 5 illustrate how THD and PF change based on α.

2) Real Power (P) and Reactive Power (Q)

Based on power transfer theory, the real power is defined as,

$$P = \frac{V_S I_1}{2}\cos\theta_1 \quad (17)$$

By putting (13) with $n = 1$ into (17), the real power equation can be rewritten as,

$$P = \frac{2V_S A}{\pi} \cdot \frac{(2\alpha-1)}{[4(\alpha-1)^2-1]\cdot(4\alpha^2-1)} \cdot 2\cos(\alpha\pi) \quad (18)$$

Based on power transfer theory, the reactive power is defined as,

$$Q = \frac{V_S I_1}{2}\sin\theta_1 \quad (19)$$

By putting (14) with $n = 1$ into (18), the reactive power equation can be rewritten as,

$$Q = \frac{2V_S A}{\pi} \cdot \frac{(2\alpha-1)}{[4(\alpha-1)^2-1]\cdot(4\alpha^2-1)} \cdot [1 - 4\alpha(\alpha-1) - 2\sin(\alpha\pi)] \quad (20)$$

III. Controller Design and Implementation

The concept of the proposed control is to keep the zero crossing points of grid current and voltage to be the same, but it carries reactive power. The ideal grid current waveform was shown in Fig. 2. Since the zero crossing points are the same as those of grid voltage, this same reference can be applied to various types of inverter to inject reactive power into the grid.

Fig. 6 (a) and (b) show two typical grid-tie inverters, an unfolding inverter and a unipolar switching full-bridge inverter, respectively. The typical gate signals of two converters are identical, SA and SB switch with the line frequency, e.g. 60 Hz, and S1and S2 switch at a high frequency, e.g. 16 kHz, to shape the inductor current. It is well known that these inverters cannot delivery reactive power or generating considerably large switching losses under standard controllers. By using the proposed technique, these topologies do not require to change any hardware components. In fact, it is only required to add a current reference generator in the control loop to produce the QSW current reference.

Fig. 7 (a) is a typical control diagram for inverters in Fig. 6 with no reactive power control [19]. The current reference is a sinusoidal waveform which is generated by a Phase-Locked-Loop (PLL) with a synchronization of grid voltage and sometimes it senses the grid voltage directly. Fig. 7 (b) shows the proposed controller block diagram, where QSW current reference generator has been introduced. The dash-line blocks illustrate the modifications of the original control loop. Firstly, a QSW reference generator replaces the simple sinusoidal wave generator. There are two parts in the generator, a sinusoidal wave generator and a controller to transform sinusoidal wave into the QSW. The sinusoidal wave generator gives a sinusoidal wave which is synchronized with the grid voltage through a PLL. Therefore, based on this signal doing some transformation to generate QSW current reference can promise the output QSW current well synchronized with the grid voltage. Secondly, as shown in blue block, for the feed-forward control, original grid voltage should also be processed to QSW shape.

The transformation from a pure sinusoidal wave to QSW only is a simple process. Firstly, based on the value and the slope of a sinusoidal wave, the phase information, ωt, can be obtained by using inverse trigonometric computation. Accordingly, a new function (23) is obtained which is transformed from Eq. (1), a QSW reference waveform can be generated.

$$f(t)=\begin{cases}-\mathrm{A}\sin\frac{\omega t+\pi}{2\alpha}, & -\pi\le\omega t<-(1-\alpha)\pi\\ \mathrm{A}\sin\frac{\omega t}{2(1-\alpha)}, & -(1-\alpha)\pi\le\omega t<0\\ \mathrm{A}\sin\frac{\omega t}{2\alpha}, & 0\le\omega t<\alpha\pi\\ -\mathrm{A}\sin\frac{\omega t-\pi}{2(1-\alpha)},, & \alpha\pi\le\omega t<\pi\end{cases} \tag{23}$$

Trigonometric and inverse trigonometric computation can be performed accurately and quickly by any DSP or micro-controller in real time.

The 2-pole 2-zero controller shown in Fig. 7 is a PID controller. Steady state error can be reduced to almost zero by selecting proper controller parameters. Controller transfer function used in this experimental test for 52 μs sampling time can be written as,

$$T_{2P2Z}(z)=\frac{-0.398z^2+0.1314z+0.5253}{-0.01z^2+1.01z+1} \tag{24}$$

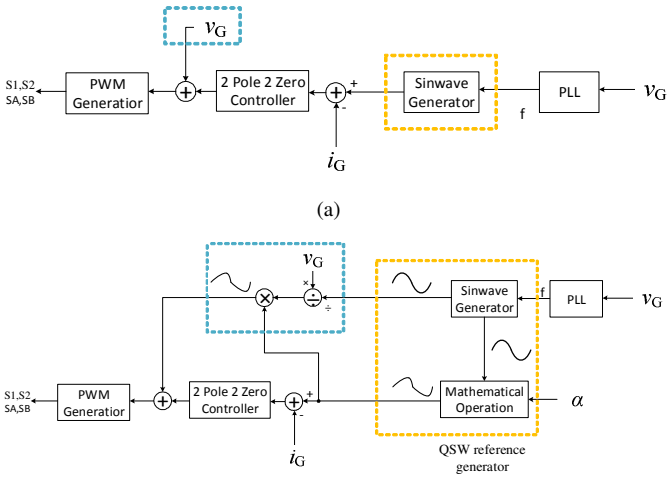

Fig. 7 Control block diagrams: (a) A typical inverter controller, and (b) controller implementation to guarantee a QSW grid current.

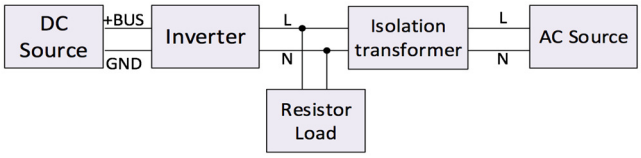

Fig. 8 Experimental test connection diagram.

TABLE I. SPECIFICATION

Parameter	Value	Parameter	Value
V_G	120V	V_{DC}	380V
P_O	400W	f_{SW}	6kHz
L_1, L_2	2.5mH	C_{AB}	10uF

IV. Experimental Verifications

The performance of the proposed controller has been experimentally demonstrated in a prototype of a full-bridge inverter. For the inverter we use a Texas Instruments (TI) solar inverter prototype, which is a full-bridge inverter with topology shown in Fig. 6 (b), controlled by a TI C2000 DSP [20]. Table I shows the specification of this inverter. In the testbed, DC source voltage is set to be 380V as input voltage of the inverter, AC voltage source which represents grid to be 110V and the peak value of QSW current reference is 5A. Fig. 8 shows the connection diagram of experimental test setup. Fig. 9 shows the waveforms of grid current when α is set at 0.22, 0.5 and 0.78.

According to Eq. (16) and Fig. 5, when α is set to 0.22, 0.5 and 0.78, theoretically the power factor should be 0.95, 1.0 and 0.95, respectively. Table II shows the measured results which are based on the current waveforms and voltage waveforms in Fig. 9. It shows that the measured power factors are very close to the theoretical results. Besides the waveforms show that the proposed control method has the ability to produce an expected QSW current which is well synchronized to grid voltage, and the zero-crossing points of grid voltage and QSW current are accurately locked.

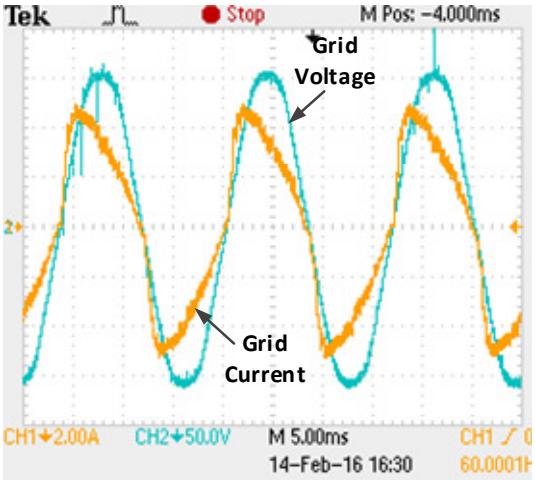

(a)

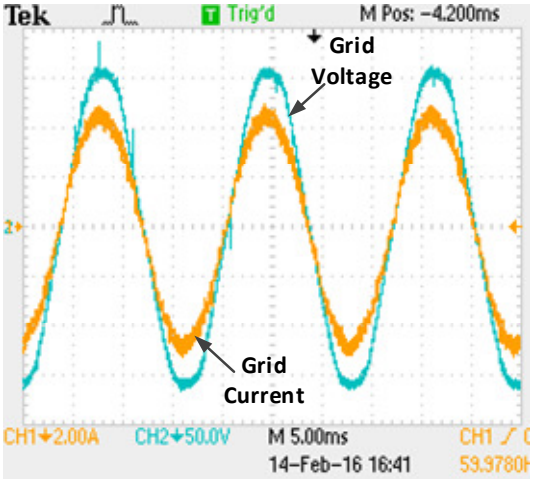

(b)

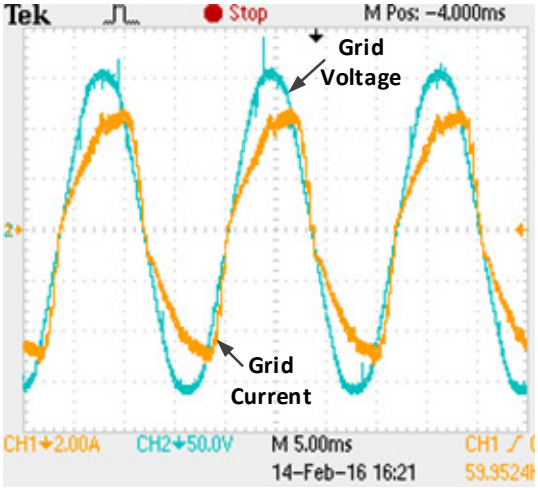

(c)

Fig. 9 Steady state responses of delivered grid current and grid voltage for different values of α: (a) $\alpha = 0.22$, (b) $\alpha = 0.5$, and (c) $\alpha = 0.78$.

TABLE II. EXPERIMENTAL RESULTS

α	Apparent Power	Active Power	Power Factor
0.22	388.7VA	371.6W	0.956
0.50	379.6VA	377.4W	0.994
0.78	371.6VA	349.8W	0.941

TABLE III. COMPARISON OF HARMONIC MAGNITUDES

	1st	3rd	5th	7th	9th
Theoretical value (A)	4.918	0.797	0.361	0.172	0.075
Measured value (A)	4.842	0.768	0.383	0.175	0.089

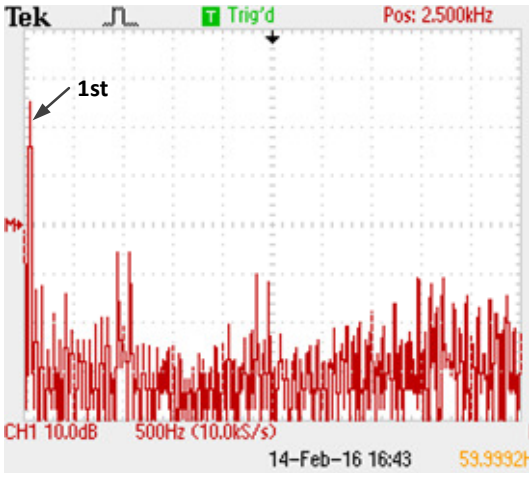

(a)

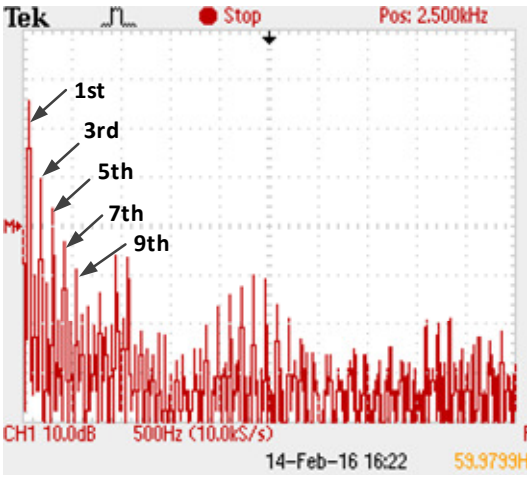

(b)

Fig. 10 Harmonic analysis, FFT of test QSW current when (a) $\alpha = 0.5$, (b) $\alpha = 0.78$.

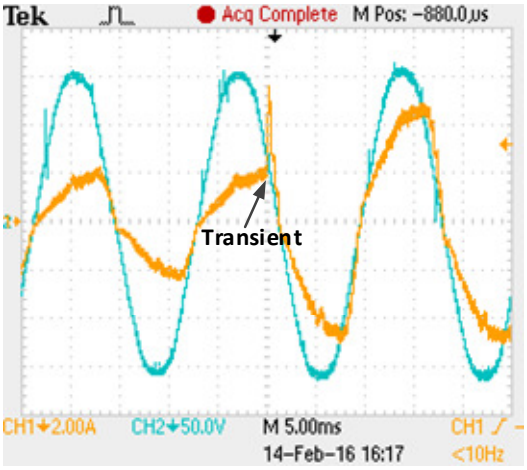

Fig. 11 Transient characteristic when $\alpha = 0.78$ and current magnitude changes from 2A to 5A.

Fig. 10 shows the FFT of test results corresponding to Fig. 9(b) that $\alpha = 0.5$ and Fig. 9(c) $\alpha = 0.78$. It can be seen that, when set $\alpha = 0.5$, the fundamental current is dominating in the frequency spectrum, it means it is very close to a pure sinusoidal wave. In contrast, when $\alpha = 0.78$, it contains extra 3rd, 5th, 7th and 9th harmonics. Table III shows the comparison of measured harmonic magnitude and theoretical harmonic magnitude calculated by (5) and (6). The comparison shows that experimental value is very close to theoretical value. For $\alpha = 0.78$, THD measured by power analyzer is 0.192, approximately satisfy Fig. 4.

Fig. 11 shows the transient characteristic of the inverter using proposed controller. At certain delay time after starting, current magnitude parameter changed from 2A to 5A. As shown, the transient happened at the current peak position which represents a worst case. However, the inverter returns to steady-state quickly with a slight overshoot, while the zero-crossing points are still accurately locked.

V. Conclusions

This paper presented a control technique for single phase unfolding grid-tie inverters. The control technique allows reactive power injection to unfolding topologies, which were limited to unity power factor operation. The idea was to provide a Quasi Sinusoidal Waveform as a grid current reference to inject reactive power. The mathematical models were provided and explained. A prototype of a unipolar switching full-bridge inverter was built. Working principle of new controller was explained. By comparing measured values and theoretical values, experimental results showed a good agreement with the theory. It was shown that reactive power injection is possible by generating quasi sinusoidal waveform current through the inverter, without changing any hardware components.

References

[1] S. B. Kjaer, J. K. Pedersen, and F. Blaabjerg, "A review of single-phase grid-connected inverters for photovoltaic modules," *IEEE Trans. on Ind. Appl.*, vol. 41, no. 5, pp. 1292 – 1306, Sept. 2005.

[2] Z. Zhao, M. Xu, Q. Chen, J.-S. Lai, and Y. Cho, "Derivation, analysis, and implementation of a boost–buck converter-based high-efficiency PV inverter", *IEEE Trans. on Pow. Electron.*, vol. 27, no. 3, pp. 1304 – 1313, Mar. 2012.

[3] U. Prasanna, and A. Rathore "Current-fed interleaved phase-modulated single-phase unfolding inverter: analysis, design, and experimental results," *IEEE Trans. on Ind. Electron.*, vol. 61, no. 1, pp. 310 – 319, Jan. 2014.

[4] Z. Yang and P. C. Sen, "A novel switch-mode DC-to-AC inverter with nonlinear robust control," *IEEE Trans. on Ind. Electron.*, vol. 45, no. 4, pp. 602-608, Aug 1998.

[5] M. A. De Rooij, and J. S. Glaser, "High efficiency, multi-source photovoltaic inverter", *US Patent* US7929325 (B2), 2011-04-19.

[6] X. Li and A. K. S. Bhat, "A Comparison Study of High-Frequency Isolated DC/AC Converter Employing an Unfolding LCI for Grid-Connected Alternative Energy Applications," *IEEE Trans. on Pow. Electron.*, vol. 29, no. 8, pp. 3930-3941, Aug. 2014.

[7] B. Sahan, S. V. Araújo, C. Nöding and P. Zacharias, "Comparative Evaluation of Three-Phase Current Source Inverters for Grid Interfacing of Distributed and Renewable Energy Systems," *IEEE Trans. on Pow. Electron.*, vol. 26, no. 8, pp. 2304-2318, Aug. 2011.

[8] P. T. Krein, R. S. Balog, and X. Geng "High-frequency link inverter for fuel cells based on multiple-carrier PWM", *IEEE Trans. on Pow. Electron.*, vol. 19, no. 5, pp. 1279 – 1288, Sept. 2004.

[9] A. K. S. Bhat and S. D. Dewan, "Resonant inverters for photovoltaic array to utility interface," *IEEE Trans. on Aerospace and Electronic Systems*, vol. 24, no. 4, pp. 377-386, July 1988.

[10] C. Rodriguez and G. A. J. Amaratunga, "Long-Lifetime Power Inverter for Photovoltaic AC Modules," *IEEE Trans. on Ind. Electron.*, vol. 55, no. 7, pp. 2593-2601, July 2008.

[11] Z. Zhao, M. Xu, Q. Chen, J. S. Lai and Y. Cho, "Derivation, Analysis, and Implementation of a Boost–Buck Converter-Based High-Efficiency PV Inverter," *IEEE Trans. on Pow. Electron.*, vol. 27, no. 3, pp. 1304-1313, March 2012.

[12] VDE-AR-N 4105, Generators connected to the low-voltage distribution network, 2011.

[13] "Steca 3600" *Photon – The Solar Power Magazine International*, 9-2011.

[14] G. Escobar, N.M. Ho, and S. Pettersson, "Method and apparatus for controlling a grid-connected converter", *US Patent* US8929108 (B2), 2015-01-06.

[15] T. Weissenhorn, D. Kloos, A. Winter, and Dirk Schekulin "Step-down-converter, DC-AC-converter assembly and method for operating the same", *EU Patent* EP2421135A2, 2012-02-22.

[16] G. James, "Chapter 4 - Fourier Series", Advanced Modern Engineering Mathematics, 2nd Edition, Addison-Wesley, 1999.

[17] S.-I. Jang and K.-H. Kim, "An islanding detection method for distributed generations using voltage unbalance and total harmonic distortion of current," *IEEE Trans. on Pow. Del.*, vol. 19, no. 2, pp. 745-752, April 2004.

[18] C. A. Canesin and I. Barbi, "Analysis and design of constant-frequency peak-current-controlled high-power-factor boost rectifier with slope compensation," *APEC '96. Conference Proceedings*, 1996, pp. 807-813 vol.2.

[19] S. Yang, Q. Lei, F. Z. Peng and Z. Qian, "A Robust Control Scheme for Grid-Connected Voltage-Source Inverters," *IEEE Trans. on Ind. Electron.*, vol. 58, no. 1, pp. 202-212, Jan. 2011.

[20] V. Xue, "High-Voltage solar inverter dc-ac kit," Texas Instruments Application Report, SPRABR5–July 2013.